batteries

MDPI

Article

Cleaning and Cross-Contamination in Continuous Twin-Screw Extrusion of Battery Slurries

Kevin Raczka, Furkan Öksüz, Nooshin Galahroudi, Emma Schiessl, Hermann Nirschl and Frank Rhein *

Institute of Mechanical Process Engineering and Mechanics, Karlsruhe Institute of Technology (KIT), Strasse am Forum 8, 76131 Karlsruhe, Germany; kevin.raczka@kit.edu (K.R.)
* Correspondence: frank.rhein@kit.edu

Abstract

In the current industry standard of batch processing electrode slurry, manual cleaning processes pose significant challenges due to their labor intensive nature. The long-term objective is to expand the existing mixing process to create an intelligent, autonomous, and continuous slurry production process. This will result in a reduction in downtime and setup times, as well as an increase in the degree of automation. Additionally, the implementation of complex parameter selection in the mixing process is intended to make it manageable for variable recipes, ensuring efficient, resource-saving process control. This study aims to address this issue by investigating the continuous production of anode slurry and its subsequent cleaning in a laboratory extruder, with a focus on optimizing the cleaning conditions and analyzing the residual slurry. Several samples were taken during the cleaning of the process area and analyzed by UV-Vis spectroscopy, while also quantifying the residual slurry on the screw elements. The effectiveness of the cleaning was evaluated using Sinner's Circle parameters, i.e., the effects of time, mechanical, chemical and thermal treatment on the effectiveness of the cleaning process are evaluated and discussed. Several detergents were tested, including deionized water, alcohol, and industrial detergents. Deionized water proved to be the most effective in terms of cleaning rate and residual slurry. In addition, higher screw speeds and flow rates improved cleaning efficiency. The effect of temperature was significant, with better cleaning rate results at higher temperatures. This indicates that mechanical and thermal factors play a critical role in improving cleaning kinetics. For a more in-depth knowledge of the resulting cell chemistry, successive cross-contamination of cathode materials in anode half-cells was examined. As a result, an indicator was identified in the first cycle that displays a voltage increase during delithiation with regard to electrochemical properties.

Keywords: cleaning; extruder; slurry processing; sinner circle; cross-contamination

Received: 6 November 2025
Revised: 10 December 2025
Accepted: 15 December 2025
Published: 18 December 2025

Citation: Raczka, K.; Öksüz, F.; Galahroudi, N.; Schiessl, E.; Nirschl, H.; Rhein, F. Cleaning and Cross-Contamination in Continuous Twin-Screw Extrusion of Battery Slurries. *Batteries* **2025**, *11*, 464. https://doi.org/10.3390/batteries11120464

1. Introduction

The demand for lithium-ion batteries has soared, driven by the rapid growth of the electric vehicles market, portable electronics, and renewable energy storage systems [1]. Although production technology requires a significant increase, transferring to production standards remains challenging. Therefore, a thorough understanding of the interactions and future pilot-scale applications is necessary. Furthermore, optimization is needed in cell production, modules, electrode design, process–structure–performance relation, cell quality, and production costs. In terms of production costs, 70% are material costs and 30% are battery production costs [2].

Regarding the production process of lithium-ion batteries, the mixing step significantly impacts subsequent steps, affecting product properties such as performance, service life, and slurry processability [3,4]. Many studies have investigated the mixing process in terms of dispersion quality [5], the influence of the conductive agent [6–8], and the process parameters in relation to the quality parameters of the slurries for different material systems [9–11]. Furthermore, simulations are also available to describe the dispersion process of the conductive agents and the properties in relation to particle sizes and electrode properties [12].

The current state of the art is the production of electrode slurries through a batch process, which severely limits flexibility and modularity. To address this issue, continuous mixing of electrode slurries with twin-screw extruders is becoming increasingly favorable as it has been proven to achieve better dispersion and deagglomeration, as well as higher cell performance and electrode conductivity [13,14]. Numerical simulations reveal intricate dependencies between shear rate, energy input, material distribution, residence time, and particle distribution [15,16]. Additional approaches to material traceability for the purpose of analyzing product consistency and initial models for describing the flow are in existence [17,18]. Moreover, automated control processes [19,20] and artificial intelligence modeling [21,22] are current research foci. In addition to increased flexibility and scalability due to its modular design, continuous processing offers further advantages in terms of process stability, degree of automation, consistent product quality, increased throughput, reduced investment, and operating costs, without negatively impacting subsequent battery production steps [3,23].

Using one extruder to process both anode and cathode materials allows for additional savings in investment costs. However, thorough cleaning is required to prevent cross-contamination. Currently, no international standard is available for cleaning electrode slurries, unlike the well-established cleaning requirements in the food, pharmaceutical, and biotech industries [24]. Current practices in batch processing rely predominantly on manual cleaning methods, which are not only time consuming but are also prone to inconsistencies and inefficiencies. Although the modular design of the twin screws can be adapted to enable a self-cleaning effect [25], there is a daunting lack of research and consensus needed for finding an optimal cleaning strategy to making the advantages offered by CIP (cleaning-in-place) a reality in battery production lines.

To ensure high quality of the battery slurry, it is essential to prevent cross-contamination, which can have serious consequences for the produced batteries, such as loss of performance or reduced battery life [26]. Possible degradation mechanisms include particle fracture, lithium plating, SEI (Solid Electrolyte Interphase) layer growth or structural decomposition [27]. It is particularly important to remove all residual particles from the processing area, especially during the transition from cathode to anode. In this regard, initial analyses of defects were carried out, which examined manufacturing defects caused by production flaws and raw material impurities. These impurities accelerate battery degradation and frequently cause internal short circuits in lithium-ion batteries [28,29]. Furthermore, the influence of electrolyte contamination on pouch cells was investigated in [30], and Li plating simulations were carried out in [31].

The aim of this work is to systematically investigate the continuous cleaning process of twin-screw extruders for minimizing cleaning time and cross contamination. A standard water-based anode slurry formulation is produced and characterized with respect to rheology and particle size distribution to establish the initial condition prior to cleaning. Cleaning kinetics are then determined by quantifying both the slurry concentration in the extruder outlet and the residual slurry in the extruder chamber. The analysis is based on the Sinner Circle, which evaluates cleaning efficiency through time, mechanical and chemical

action, and temperature, complemented by contamination type and surface geometry [32]. On this basis, cleaning instructions for the extrusion plant after anode slurry production are developed. Different cleaning media, as well as flow rate and screw speed, are systematically assessed, given that effective removal of residues is essential for consistent slurry quality. To verify the remaining contamination and its influence on subsequent processing steps, a detailed analysis of successive contamination is performed. Cathode materials were mixed into anode slurries, and the resulting anode half-cells were cycled to determine the impact of potential contamination during the mixing step. Electrochemical analyses detected contamination right at the start of cycling.

2. Materials and Methods

This section comprises the materials and methods used to produce, analyze and test the cleaning of the anode slurry. A detailed presentation of the materials used is given, as well as a description of the specific procedures and equipment used for these processes. Due to their inexpensive and more sustainable properties, an increasing number of cleaning tests have been carried out using anode materials in order to gain as much knowledge as possible about the various cleaning processes in the extrusion process.

2.1. Materials for Slurry Production

The anode slurry consists of the main components active material, conductive additive, binder and solvent. In order to ensure comparability of the test results of the cleaning processes, a standard recipe was used for the production of the anode slurry. This formulation has a liquid content of 55 wt% and a solid content of 45 wt%. The same formulation was used for all experiments, containing 93 wt% anode active material (graphite), 2 wt% carbon black (CB), 2 wt% carboxymethyl cellulose and 3 wt% styrene-butadiene rubber (SBR) for li-ion battery anodes. Deionized water was used as solvent.

In this work, MECHANO-CAP©1P1 was used as the anode active material, which is a high-purity, spherical natural graphite produced by the Mechanodesign process. This process ensures accessibility of the basal planes of the graphite, which are planar layers of carbon atoms, allowing rapid intercalation and deintercalation. C-NERGY SUPER C65 Conductive Carbon Black from Nanografi Nanotechnology was used as the conductive carbon black due to its high electrical conductivity and low density. Of particular importance is the low specific surface area of 62 m^2/g, which allows for uniform distribution of the conductive additive in the solvent. However, it should be noted that CB tends to agglomerate in aqueous solvents, which reduces conductivity and can affect the homogeneity of the anode slurry. The binders used are CMC powder with a degree of substitution of 0.8 from Carl Roth and SBR from Nanografi Nano Technology which is a milky white liquid emulsion and has a solid content of 51.3%. This combination provides effective binding and stabilization of the anode materials, thereby improving the mechanical flexibility and adhesive strength of the anode.

The variation in the recipe significantly affects the resulting slurry, and the conductive agent and binders are essential for the processability of the slurry. The choice of CMC binder, in terms of its molecular weight and degree of substitution, is crucial for adsorption onto graphite particles. This affects not only the flow behavior and processability of the slurry, but also the microstructure of the dry layers, as well as their electrical conductivity and cohesive strength [33]. For reproducibility purposes, the same formula was selected in the first step despite its effects on the subsequent cleaning process. This was done to obtain a detailed analysis of the cleaning process.

2.2. Detergents

Based on preliminary turbidity tests for cleaning anode slurries in a continuous process, the following cleaning agents were evaluated to determine their cleaning effectiveness for removing slurry residues from the screws of the twin-screw extruder: Deionized water was used as the primary cleaning agent because it allows thorough cleaning and removal of water-soluble residues without leaving behind minerals or salts. It also serves as the solvent for making the anode slurry. The water has a residual conductivity of 5 µS/cm and a pH of 7.

Ethanol (99.9%, CAS 64-17-5, Häffner GmbH, Asperg, Germany) is investigated as detergent as it is completely miscible with water and many organic solvents and its relatively low viscosity. However, its use in industrial applications requires explosion protection certificates, which makes its use in larger cleaning processes more complicated. The Industrial Cleaner CB-100 from Bio-Circle Surface Technology GmbH is a highly effective cleaning agent specially developed for the removal of residues in plastics and polymer processing. As an aqueous and low-foaming cleaner, CB-100 is based on renewable raw materials and is therefore environmentally friendly and biodegradable. It is designed to effectively dissolve and remove polymer deposits, dirt, grease and other stubborn contaminants, including soot and rubber residue, making it interesting in the scope of this work.

Finally, Ecolab's (Monheim am Rhein, Germany) COSA™ CIP 96 was used, a highly alkaline, surfactant-free, sequestering cleaner designed for clean-in-place (CIP) cleaning in pharmaceutical processing equipment. It is particularly suitable for the removal of fat and protein-containing residues. When selecting the cleaning media, special attention was paid to operation at room temperature, as elevated temperatures must be avoided at all costs when using certain formulations and solvents due to the possible risk of ignition. The aim is to find a general procedure that can be used universally. Cleaning granules from the company ver-rus were also studied in more detail, as reported in the presentation of results. These are cleaning concentrates consisting of plastics and require a relatively high temperature to effectively remove deposits and contaminants in plastic processing machinery.

2.3. Continuous Production and Cleaning Procedure

Premixing and homogenizing the respective powders is essential to ensure a homogeneous slurry of the appropriate quality. A JEL RRM Mini-II rotary mixer with a maximum filling volume of 5 L was used in this setup. This mixing process took place for over an hour at a tumbling speed of 40 rpm. The free fall mixing method ensures a homogeneous distribution of the components regardless of their proportions or particle sizes.

A Thermo Fisher Scientific Inc. (Waltham, MA, USA) Energy 11 co-rotating twin-screw extruder was used to process and clean the anode slurries to compare the cleaning procedure after each production step. The extruder used screws with a diameter of 11 mm and a process length with an L/D ratio of 40:1. The entire extruder was housed in an MBRAUN LABmaster pro GloveBox. This GloveBox was filled with argon gas to prevent unwanted oxidative reactions and wetting of the powder mixture.

The extruder can reach screw speeds of 10 rpm to 1000 rpm, which allows precise control of the mixing process. There are seven cooling and heating zones to control the temperature during extrusion. Figure 1 shows the setup of the applied screw configuration, which was used to produce the anode slurry and consecutive cleaning in the same process chamber. The screw configuration consists of three conveying zones and two kneading zones. The kneading zones of the selected cleaning configuration consist of eight and ten mixing elements with a 60° offset and three additional mixing elements with a 30° offset. A liquid feed is provided first, followed by a powder feed in the next zone. To

improve powder metering and conveying, two push-screw elements, each twice as long as conventional conveying elements, were used. The liquid was supplied by a Masterflex Easy Load II 77200-60 pump, which allows flow rates of 0.06 mL/min to 2300 mL/min and speeds of 1 rpm to 600 rpm, ensuring precise dosing of the liquid components directly into the screws and thus a uniform mixture.

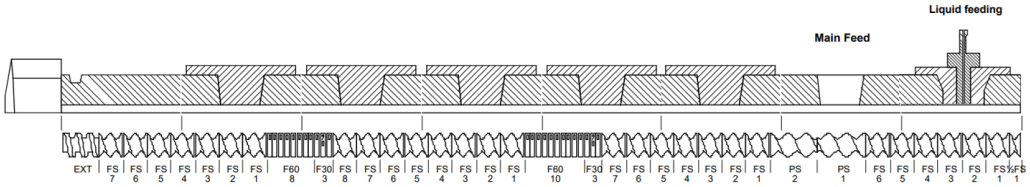

Figure 1. Schematic representation of the cleaning screw configuration and casing of the laboratory extruder with the liquid supply in the first zone and the powder supply in the second (from right to left). The initials FS (feed screw) and PS (push screw) describe the respective conveying elements. The mixing elements are characterized by F60 and F30, which have an offset of 60° and 30° to each other per element.

After the anode slurries were produced, systematic cleaning tests were conducted to evaluate the efficiency of various cleaning media. The extruder was rinsed with various cleaning agent which means that the pump fed the respective liquid via the liquid feeding in Figure 1 while the extruder was running at a certain screw speed. The process parameters, including screw speed, cleaning agent flow rate, and temperature zones, were examined for an in-depth analysis that is referred to and described accordingly in the following chapters. In addition to chemical and time analysis, these adjustable parameters provided a comprehensive insight into the mechanical cleaning component. The cleaning process started with rinsing the extruder with the appropriate cleaning medium. Samples were taken as soon as the cleaning medium reached the extruder outlet, and further samples were taken after one, three, five and ten minutes. This ensured comparability over a cleaning time of ten minutes in order to study the cleaning kinetics in more detail. The process was conducted in triplicate and the standard deviation between repetitions was computed to assess reproducibility.

Following anode slurry production and cleaning, the screws were pulled and cleaned in an ultrasonic bath to thoroughly remove any residual slurry remaining on the screws. A transsonic ultrasonic bath operating at a frequency of 130 kHz was used. The screws were placed in the ultrasonic bath for 15 min. Ultrasonic cleaning allows for the effective removal of contaminants. This made it possible to completely clean the complex surfaces and structures of the screws. On the one hand, this was necessary to determine the amount of residual slurry remaining on the screws, which is of great importance for assessing the quality of the cleaning. In addition to the cleaning kinetics in the process chamber, the amount of remaining slurry on the screws is also critical. This amount has been measured gravimetrically.

2.4. Quality Control of Anode Slurry

In order to better understand the studies on the purification of the anode slurry, the respective quality parameters of the anode suspension were determined for the recipe already described in Section 2.1. These are the rheological properties of the slurry as a function of speed and the respective particle size distributions.

The rheological properties of the anode slurries were measured and analyzed using a Thermo Scientific™ HAAKE™ Viscotester™ iQ Rheometer. To determine the viscosity, the dynamic viscosity η is plotted against the shear rate $\dot{\gamma}$ as the behaviour is structurally viscous. The shear rate range is 0.01/s to 1000/s. A plate-plate rheometer with a gap

height of 0.5 mm is used. The plate has a diameter of 35 mm and was always measured at a constant temperature of 20 °C.

Particle size distribution is determined using a Mastersizer 3000 laser diffractometer (Malvern Panalytical GmbH, Kassel, Germany), which is a sequential combination of red and blue light source measurements, and a 120 mL Hydro MV wet dispersion unit. The sample dispersion unit ensures that the particles enter the measuring range of the optical bench at the correct concentration and in an appropriate stable dispersion state to ensure accurate, reproducible measurements. In this application, the anode suspension was successfully measured at a dilution of 1:100. The measurement range of the particles is from 10 nm to 3.5 mm in width, measured by angular scattering intensity. While the large particles scatter light at a small angle relative to the laser beam, the small particles scatter light at a large angle.

In order to optically assess the structure and network of the anode slurry, SEM images were recorded. For this purpose, the slurry produced was manually applied to a copper foil using a squeegee. The coating thickness of the electrode was 100 µm and the thickness of the copper foil was 10 µm. The coated electrode was then dried and prepared accordingly. For this purpose, samples from the electrode layer were punched out and SEM images were taken of the top side of the electrode for different size scales.

2.5. Concentration Analysis

In order to assess the effectiveness of the cleaning processes, it is necessary to determine the mass fraction of the anode slurry in the cleaning samples taken. This makes it possible to determine the temporal evolution of the mass fraction during the cleaning process over a total of ten minutes, which allows a comparison of the cleaning processes carried out in terms of their efficiency and effectiveness. This procedure is based on the washing ratio for filter cakes, which uses continuous flow and dilution methods [34]. Concentrations were determined using UV-Vis spectroscopy, an analytical technique that examines the absorption of ultraviolet (UV) and visible light (VIS) for various substances. A Flame-S UV-Vis spectrometer from Ocean Insight was used for the UV-Vis spectroscopy. The detector used in the FLAME UV-Vis spectrometer covers a wavelength range from 190 nm to 1100 nm. The optical resolution is typically 0.1 nm to 10 nm, which allows precise measurement of absorption and transmission [35]. In addition, a deuterium-tungsten-halogen light source is used to cover the spectrum in the UV and visible regions.

A UV-Vis spectrum is a list of wavelength-specific absorbance values. The Lambert–Beer law establishes a linear relationship between the absorbance A and the concentration of the substance c. Taking into account the molar mass M and density ρ, this concentration is converted into a mass fraction w. Hence, the relationships for determining the mass fraction in the cleaning samples is given by

$$w = \frac{M}{\rho} \cdot \underbrace{\frac{1}{d \cdot \varepsilon_\lambda} \cdot A}_{Lambert-Beer} \tag{1}$$

where d corresponds to the path length of the light through the sample and ε_λ to the absorption coefficient. The latter is a substance-specific quantity and describes the absorption strength of a substance at a specific excitation wavelength λ. The absorption coefficient ε_λ, the density ρ and the molar mass M are introduced as unknowns. However, the linear relationship between mass fraction w and absorbance A can be determined from Equation (1) using linear regression. After measuring certain samples of known mass fraction, a calibration curve is obtained, that allows for the analysis of the mass fractions of the cleaning samples [35]. The reference data was generated using 10 g of anode slurry with

a solids content of 45%. This slurry was diluted in ten steps at a ratio of 1:1. All diluted samples were measured tenfold by UV-Vis spectroscopy and the average absorbance values are visualized over the wavelength in Figure 2a. Water was used as a reference sample and nine further diluted slurry suspensions were included in order to use the maximum measurement interval with the highest accuracy.

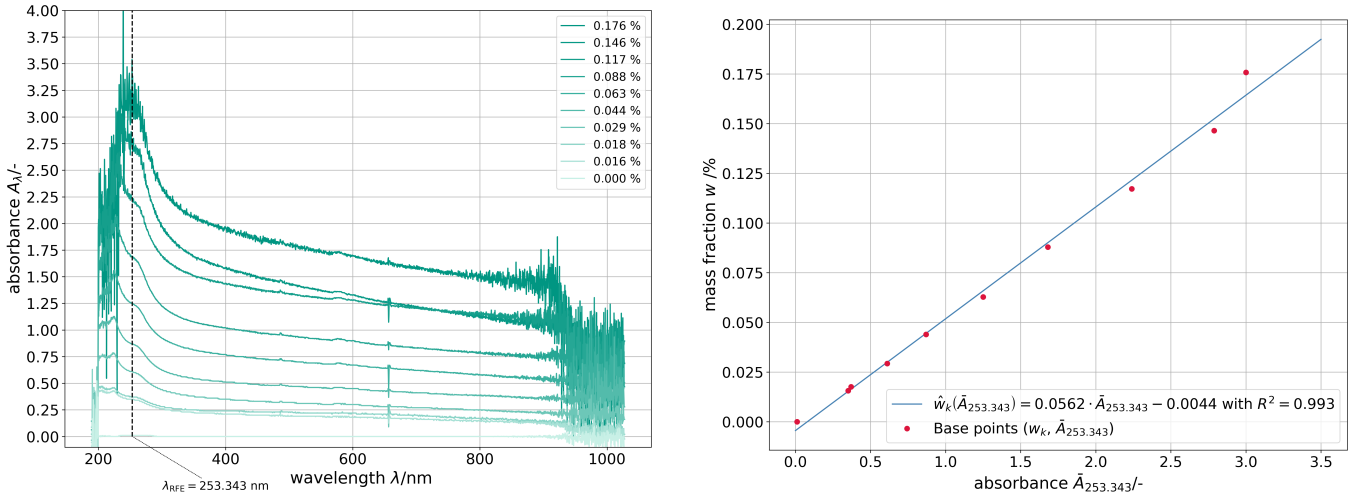

(**a**) (**b**)

Figure 2. Preliminary calibration to determine the cleaning results using UV-Vis spectroscopy. (**a**) Absorption spectra of the diluted solutions as a reference in dependence of the wavelength. (**b**) Linear calibration curve of the mass fraction as a function of the absorbance.

The wavelength to construct the calibration curve was chosen at 253 nm by Recursive Feature Elimination (RFE). Here, multivariate models are trained on all wavelengths and in each iteration, the wavelengths with the smallest regression coefficients are removed until only the desired number of features—in this case one—is left. This prevents overfitting of the model and yields the most robust prediciton of concentration. The calculated calibration curve is shown in Figure 2b. The data points clearly show the linear relationship between the measured absorbance and the mass fraction. The constructed regression line has a coefficient of determination of 0.993, indicating a very good agreement between the observed and predicted values. As can be seen in Figure 2a, too high absorbance values result in noise. Therefore, all experimental samples were diluted to an absorbance value smaller than 0.2.

2.6. Electrode Manufacturing and Analysis

To better evaluate the slurry structure, the anode suspensions produced were applied to a copper foil using a squeegee process with a gap height of 100 µm. In order to gain a qualitative understanding of the electrode microstructure, SEM analyses with the Gemini SEM from Carl Zeiss, Germany were conducted. The SEM was operated at an acceleration voltage of 5 kV. The electrical properties of the electrode were determined using the Hioki RM2610 system, which combines a four-wire measurement with multi-point potential mapping and enables the extraction of both volume and interfacial resistivity.

2.7. Cell Construction and Cycling

For the purpose of obtaining an overview of the lithium-ion battery manufacturing process, it is essential to detect the influence of possible cross-contamination of cathode materials in anode production. To establish a correlation based on the initial mixing step, the final anode slurry was intentionally contaminated with the cathode materials NMC and

LFP. Specifically, these were NMC622 from BASF and LFP400 from ibu-tec. The resulting electrode slurries were coated onto copper foils, dried, and stamped to form coin cells.

Type 2032 button cells were used for this purpose. Each anode electrode has a diameter of 12 mm, and a Li metal counter electrode with a diameter of 14 mm was used. The button cells were constructed according to the following scheme: a casing bottom, an anode electrode, and the addition of 200 µL of $LiPF_6$ electrolyte with a Whatman phase separator with a 16 mm diameter. Then, the Li metal, a 1 mm thick spacer, and a spring were added, followed by the buttin lid. After compression at 650 psi, the finished cell was thoroughly cleaned before cycling. In the first cycle, each coin cell was started at C/10. After completing a full charge and discharge process, the cell was measured at C/3 for a total of 100 cycles. Voltage limits of 50 mV to 0.7 V were used for this.

3. Results

This chapter presents and analyzes in detail the results of the experiments carried out to evaluate the produced slurry in terms of the quality parameters of rheology and particle size distribution, and to clean the anode slurry in the twin-screw extruder. Emphasis is placed on the investigation of various parameters and their influence on the effectiveness of the cleaning processes. The relevant cleaning factors are summarized by the Sinner circle, which includes the chemical cleaning medium, mechanical kinetics, temperature and cleaning time. Images are also used to illustrate the most significant differences. Finally, electrochemical analysis of cross-contamination during cycling concludes the investigation of the process chain for manufacturing lithium-ion batteries.

3.1. Quality Parameters of Slurry

The quality of the produced anode slurries was determined by measuring viscosity and particle size distribution (PSD). Slurry quality is important, because it will influence the subsequent cleaning step. The viscosity curves shown in Figure 3a describe the dependence of dynamic viscosity on shear rate for different twin screw speeds. Five different screw speeds were chosen, ranging from 100 rpm to 1000 rpm. All curves confirm a structurally viscous behaviour, as the viscosity of the slurry decreases with increasing shear rate at all speeds studied. This behavior suggests that the structure of the anode slurry is more affected at higher speeds in the extruder, leading to a reduction in viscosity. The arrangement of the particles and the interactions within the slurry are affected by the shear forces, resulting in the formation of a different network between the particles and the binder [36].

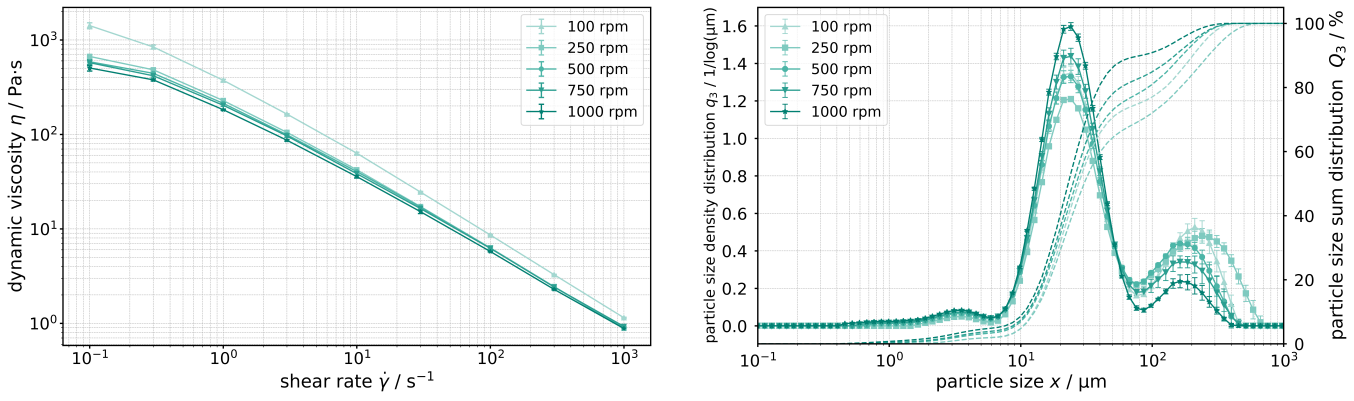

(**a**) (**b**)

Figure 3. Quality parameters of the anode slurry as a function of the screw speed used in the extruder chamber. (**a**) Viscosity curves as a function of the shear rate. (**b**) Volume-weighted density distributions of the particle sizes.

On the other hand, Figure 3b shows the particle size distribution of the anode slurry as a function of the respective particle size for different screw speeds from 100 rpm to 1000 rpm. The distribution shows three distinct peaks indicating the presence of different particle classes. The first peak, with particle sizes between 1 µm and 10 µm, represents the smaller aggregates resulting from the dispersion of the carbon black. These particles remain relatively stable even at higher speeds, indicating that they are highly agglomerated or aggregated and difficult to break up. The second peak at about 20 µm largely reflects the graphite content and the third peak at about 150 µm to 200 µm shows the presence of larger agglomerates formed by the aggregation of several aggregates. The height and width of this peak decrease with increasing speed, indicating that these larger agglomerates are broken up at higher shear forces in the extruder. The decrease in particle size distribution in the region of the larger agglomerates explains the decrease in viscosity as described in the Figure 3a.

A significantly more homogeneous distribution can be achieved by implementing a pretreatment process before homogenisation of the powders that will be inserted into the extruder chamber by the feeder, or by optimizing the process parameters. The residence time, and therefore the resulting material, can be adjusted by reducing the mass flow rate and increasing the energy input [16,37,38]. This can be achieved by using a different screw configuration or a higher extruder speed, for example [14]. However, the focus here was on investigating the corresponding cleaning process, so the same process parameters were always used for reproducibility purposes. Furthermore, it should be noted that viscosity is largely independent of PSD because the adsorption of CMC molecules significantly affects viscosity, which dominates and decides the consecutive cleaning kinetics [39].

At lower screw speeds, the slurry remains more inhomogeneous as the larger agglomerates settle more quickly. At higher screw speeds, the slurry becomes more homogeneous and stable as the agglomerates are broken up, which can be advantageous for processing. In summary, Figure 3b shows that higher screw speeds in the extruder result in better dispersion of the particles and breaking up of larger agglomerates, which in turn helps to reduce the viscosity and improve the processability of the anode slurry. The resulting quality characteristics have a critical impact on cleaning, which is highly dependent on the composition and initial viscosity of the slurry. For subsequent cleaning, the same recipe with the same solids content was used for reproducibility. The extruder throughput for production was also set to be constant at 1 kg/h of slurry and the screw speed was 750 rpm.

In order to gain a better understanding of the material being processed for consecutive cleaning, the corresponding electrode was subjected to optical examination via SEM based on the selected slurry formulation. A specific location was analyzed for different size scales, which are shown in Figure 4. The active material graphite and the conductive carbon black binder network are clearly visible in all images. The SEM micrographs at different magnifications reveal the characteristic microstructure of the graphite-based anode. At low magnification, large platelet-like graphite particles with irregular edges can be clearly identified. The particles are relatively densely packed but still exhibit interparticle voids. With higher magnification, the layered morphology of the graphite becomes more apparent, and the interfaces between adjacent particles are visible.

In the subsequent images, the surface topography of the graphite platelets is shown in greater detail. Sharp edges, steps, and fracture planes highlight the crystalline nature of the graphite domains. In addition, fine particulate material can be observed in the pores and on the surfaces of the larger platelets, which likely corresponds to conductive additives and binder residues. These features form a percolating network between the graphite particles and contribute to the electrical conductivity of the electrode.

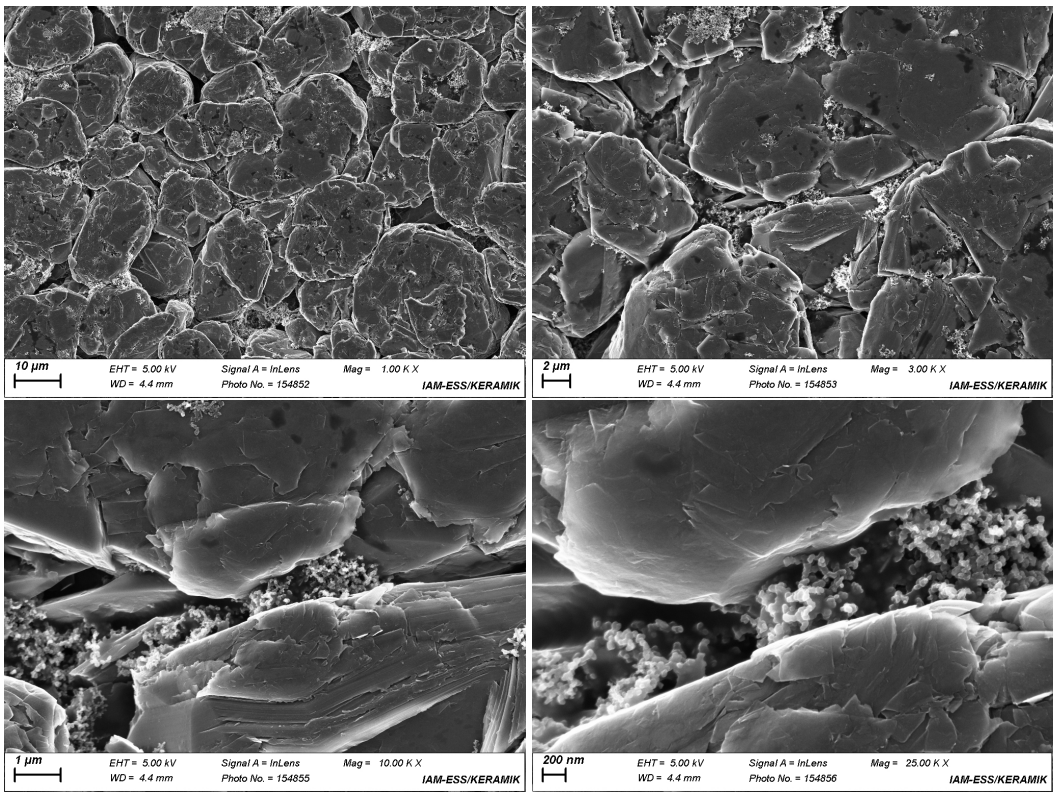

Figure 4. SEM images of the coated electrode from above. The respective anode formulation was coated on a copper foil, dried and then analyzed for various magnifications.

Furthermore, the electrical resistivity of the electrodes was analyzed. The measurement yielded a composite volume resistivity of $0.181 \pm 0.07\,\Omega\,\mathrm{cm}$, an interface resistance of $0.0347 \pm 0.0046\,\Omega\,\mathrm{cm}^2$, and a composite surface resistivity of $0.00077 \pm 0.00007\,\Omega\,\mathrm{cm}^2$. Overall, the SEM analysis demonstrates a heterogeneous but interconnected microstructure consisting of graphite as the active material, with smaller particles and binder phases distributed along the particle boundaries. The hierarchical porosity visible at different length scales indicates pathways for electrolyte infiltration while simultaneously providing sufficient electrical connectivity through the carbonaceous binder network.

3.2. Cleaning Time

The cleaning time, although one component of the Sinner circle, is not varied as a separate parameter in this work. Rather, continuous cleaning curves are obtained by measuring time-specific samples. The optimal duration must be chosen to ensure complete removal of residues without excessive consumption of resources. This is particularly important for industrial applications where both the effectiveness and efficiency of the cleaning process are of great importance. In general, all experimental investigations, which will be elaborated in more detail in the following sections, showed a reduction in slurry weight fraction with increasing cleaning time. The results generally showed that the cleaning performance is highest at the beginning of the cleaning process. With increasing time, the slope of the curve, and thus the amount of residue removed, decreases, indicating a decreasing effectiveness over time.

Most cleaning samples show that cleaning is largely complete after five minutes, which is sufficient to assess the effectiveness of the method. After ten minutes, only a small mass fraction of the anode slurry remains, indicating almost complete removal of the residues by the cleaning methods used. Further evaluation reveals two essential processes. Firstly, the

remaining suspensions are discharged, and then the residues are rinsed out. To quantify the cleaning kinetic, a double-exponential model

$$w(t) = A_1 \cdot e^{-k_1 t} + A_2 \cdot e^{-k_2 t} \quad (2)$$

is used to fit the data and describe the decrease in mass fraction w. The time-dependent concentration consists of two superimposed decay components. A_1 and A_2 represent the relative proportions of the decaying components and the initial mass fraction before exponential decay begins, whereas coefficient A_1 represents the rapidly decaying fraction associated with the fast removal of loosely bound residues, whereas coefficient A_2 denotes the slowly decaying fraction corresponding to the gradual removal of more strongly adhered or inaccessible residues. The sum of both indicates the total weight fraction of slurry at the outlet at $t = 0$, i.e., how much slurry is present at the beginning of the cleaning procedure. Note that the starting point for each measurement is different. Each measurement was taken analogously, beginning with the first drop of cleaning agent and continuing for the same time interval. Slight deviations occurred at the start of each measurement depending on the cleaning medium and process parameters, because these factors strongly influence the dwell time.

The parameters k_1 and k_2 describe the corresponding rate constants. Thus, analogous to an existing model for describing the kinetics of dispersion, a kinetic model was developed to describe the cleaning processes [40]. The rate constants primarily describe the cleaning kinetics and are referred to as the cleaning rate, which describes the cleaning speed. These parameters are crucial for determining cleaning efficiency over time. The first term in Equation (2) describes a rapid initial reduction associated with the direct displacement effect resulting from the flow of the cleaning agent and directly rinsable residues of the suspension. The second term represents a significantly slower decrease corresponding to the removal of residual adhesions or hard-to-reach contaminants. This allows cleaning processes to be compared under identical conditions with regard to cleaning kinetics.

In addition to analyzing the cleaning kinetics and the cleaning process in the process chamber, it is crucial to quantify the amount of slurry remaining on the twin screws. Complete and effective cleaning can only be guaranteed by considering the combination of both parameters, as fast cleaning does not necessarily mean complete cleaning. When studying the cleaning efficiency of various parameters, the residual slurry remaining on the twin screws after cleaning was weighed and elicited for each cleaning strategy in the respective following chapters. Finally, Section 3.6 summarizes every cleaning procedure that has been investigated in this study.

3.3. Variation of the Cleaning Agent

Cleaning tests using solvents such as ethanol, isopropanol, acetone and recommended industrial cleaners were conducted as part of initial preliminary testing. After consultation with industry experts and based on the knowledge gained, the cleaning media were narrowed down to the following for more specific investigation. Figure 5 compares the cleaning media deionized water, ethanol, COSA™ CIP 96 and CB 100 in terms of their effectiveness in removing residues from the anode slurry and shows the different cleaning kinetics. The exponential fit according to Equation (2) is also shown and the numeric value of the kinetic parameters k_1 and k_2 are provided in the legend. All fits reached high degrees of determination ($R > 0.999$) and the full data of all fit curves is provided in the Appendix A Table A1. The four detergents show different decay curves of the mass fractions over the cleaning time. Deionized water starts with a mass fraction at 6.568% and shows a rapid decrease in the first few minutes before stabilizing at a low level. This shows the high effectiveness of deionized water in removing anode slurry residues.

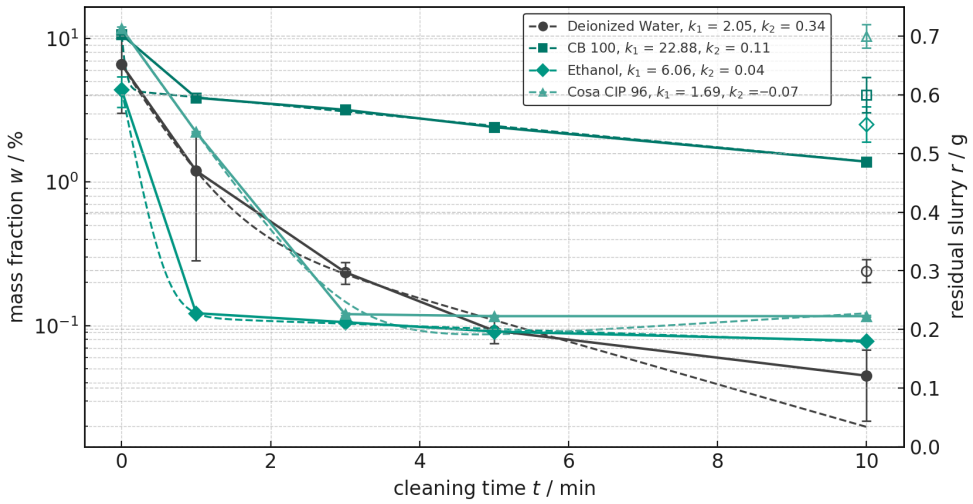

Figure 5. Influence of different cleaning media on the cleaning performance at 500 rpm and 1000 mL/h. Error bars indicate the standard deviation of triplicate cleaning experiments. Dashed lines show the fitted cleaning kinetic model.

To be noted, cleaning kinetics or model parameters alone can be misleading. In addition to long-term kinetics, the absolute values and final residual slurry in the extruder must be compared. For the final assessment, the residual slurry after each cleaning process was plotted on the second y-axis in Figure 5. This data confirms that water is the most effective cleaning medium because the residual slurry mass is lowest. While the initial ejection removes most of the slurry produced from the extruder chamber, the removal of the last particulate residues is crucial for effectiveness.

Ethanol starts at 4.376% and also shows a rapid decrease in the first few minutes, but stabilizes at a slightly higher level than deionized water. The second highest cleaning rate k_1 at the beginning of 6.234 is obtained for Ethanol. This is due to the fact that ethanol has reached its cleaning limit and only removes the superficial and easily soluble components of the anode slurry. Although ethanol lowers surface tension, it does not lower it enough to break the adhesion of binders. In contrast, water-based anode slurries are formulated to adhere well to surfaces. The less soluble components, such as graphite and carbon black, which are more adherent to the surface, remain on the screws and are not effectively removed. As a result, after about one minute of cleaning, only relatively clear ethanol flowed from the extruder outlet without a large amount of suspended slurry residue which is confirmed by a small value of 0.042 for k_2. In comparison, deionized water shows a k_2 value of 0.342, indicating much better cleaning efficiency over a longer cleaning time. Therefore, from a chemical perspective, ethanol proves to be an ineffective cleaning agent, but it emphasizes the effectiveness of the extruder in removing the remaining slurry.

COSA™ CIP 96 shows no significant change in the mass fraction of residues after 3 min, indicating that this cleaning medium is not very effective. The cleaning kinetics model also confirms this, as it yields the only negative k_2 value for this medium. The slightly negative value most likely stems from fitting and experimental errors and should be interpreted as zero, i.e., the absence of a slower, diffusion-driven deep cleaning. Graphite and carbon black are hydrophobic, carbon-based materials that are difficult to dissolve in water-based cleaners. The chemical stability and strong adhesion of these components can reduce the effectiveness of CB 100. Additionally, the low-foaming formulation, when combined with the shear forces caused by rotational speed, limits interfacial activity. This reduces the mechanical detachment required to remove fine graphite or carbon black (CB) particles, as well as the formulation's limited compatibility with CMC-based residues. This explains why CB 100 loses its effectiveness after the first minute of cleaning. Although the

cleaning rate k_1 shows the highest overall value, the absolute values of the mass fractions over cleaning time show no advantage.

In order to better assess the effectiveness of the cleaning process, Figure 6a illustrates the double screw geometry used immediately after processing the anode slurry formulation. The black slurry can clearly be seen distributed along the screw, particularly in the kneading elements and in the last section of the conveyor elements before discharge. Figure 6b–e shows the twin screws at the end of each cleaning process for visual assessment. For this purpose, the four different cleaning media were considered separately. At first glance, the screw appears clean after cleaning with CB100, but upon closer inspection, many black spots remain, indicating that they did not come off during cleaning. For the ethanol procedure, it is clear that the slurry dried more strongly on the screw elements. For this reason, ethanol is absolutely unsuitable for removing residual slurry. With COSA CIP as the cleaning medium, the screw appears very dark, which is confirmed by the cleaning performance of the measured samples.

In summary, deionized water with a high cleaning rate of k_2 has the best cleaning performance and is the most effective cleaning medium under the tested conditions. Also, there are hardly any visible residues and the screw alone shows the cleanest results based on visual assessment. Furthermore, when using water as a cleaning agent, no further impurities originating from the cleaning agent itself are to be expected that could affect the quality of the slurry. This is why further testing of process parameters was carried out with this solvent.

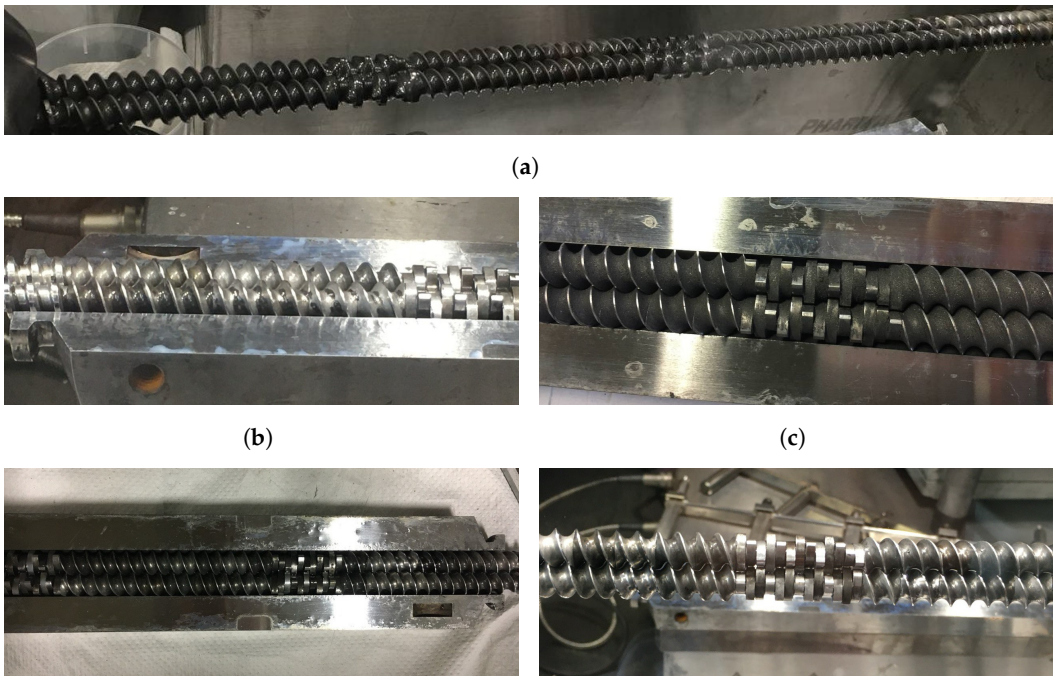

(**a**)

(**b**) (**c**)

(**d**) (**e**)

Figure 6. Visual assessment of the twin screws at the end of each cleaning process for the various cleaning media. (**a**) Reference image of the twin screws immediately after slurry processing. (**b**) CB100 as cleaning agent. (**c**) Ethanol as cleaning agent. (**d**) Cosa CIP as cleaning agent. (**e**) Water as cleaning agent.

3.4. Mechanical Investigations

In this section, the influence of various mechanical procedures on the cleaning performance is examined. The parameters considered include the change in the amount of cleaning medium to be conveyed and the screw speed of the extruder which is responsible

for the main energy input. The test results are analyzed based on the quantitative approach and the cleaning kinetics according to Equation (2).

3.4.1. Speed of Double-Twin Screws

Figure 7 shows the influence of the screw speed on the cleaning kinetic. The screw speeds 200 rpm and 1000 rpm were studied at a constant flow rate of 756 mL/h with deionized water in order to determine the two extremes of the screw speed and thus obtain information about the parameter range of the extruder. The data show that the cleaning rate of k_1 is slightly higher at higher speeds, resulting in a value of of 2.567 in comparison, but the second term shows that k_2 is much higher for lower speeds. This shows that higher screw speeds are beneficial at the beginning for better ejection, but concerning the dwell time a slower screw speed is in advantage. After ten minutes of cleaning, the mass ratio at 1000 rpm is only 0.025% compared to 0.034% at 200 rpm.

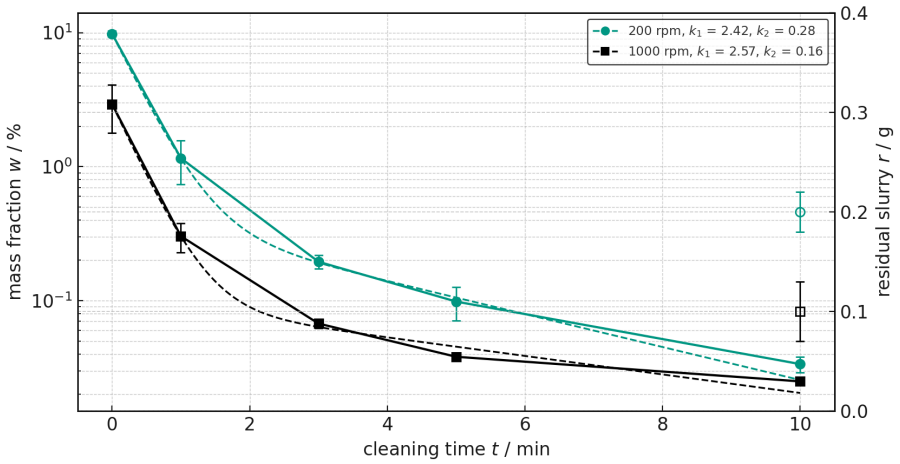

Figure 7. Influence of the speed on the cleaning performance with demineralized water at a constant volume flow of 756 mL/h. Error bars indicate the standard deviation of triplicate cleaning experiments. Dashed lines show the fitted cleaning kinetic model.

Higher screw speed creates greater shear forces and turbulence in the extruder, which helps to remove contaminants from the surface. This explains why cleaning is faster at 1000 rpm and why the mass fraction decreases faster at the beginning. For further discharge, a lower screw speed results in a beneficial cleaning rate due to less intense rotational forces, supporting the axial movement. The higher speed can also result in better mixing and distribution of the detergent, ensuring that hard-to-reach areas such as between the kneading elements are cleaned more efficiently. Furthermore, the fill level decreases as the speed increases, which has a significant impact on cleaning. Finally, a longer contact time is improving cleaning due to slower movement and longer dwell time.

The results indicate that the dynamic effects, such as increased turbulence at high speeds due to the increased shear forces, contribute significantly to the cleaning efficiency. The gravimetric validation confirm the UV-Vis spectroscopy results in Figure 7. In this evaluation as a higher screw speed leads to less residual slurry, here 0.1 g compared to 0.2 g at lower speed. This suggests that the use of higher speeds is favorable to ensure fast and thorough cleaning of the extruder. The analysis illustrates the importance of mechanical influences and flow dynamics in optimizing cleaning processes in industrial applications. The interplay between the correct speed and the volume flow of the cleaning medium is therefore crucial for the cleaning kinetics and effectiveness.

3.4.2. Volumetric Flow Rate of Cleaning Agent

Figure 8 illustrates the influence of the volume flow rate for three different flow rates (304 mL/h, 504 mL/h and 704 mL/h) on the cleaning performance at a constant extruder speed of 500 rpm. It can be observed that a higher flow rate improves the cleaning efficiency as cleaning rate and effectiveness of the remaining slurry are favoring. After ten minutes of cleaning, the mass ratio dropped to 0.015% at a flow rate of 704 mL/h, while it was still 0.042% at 304 mL/h. This indicates that increasing the flow rate accelerates the removal of residuals because the cleaning medium flows faster through the extruder, rinsing out more potential contaminants.

The average residence time is shorter for processing in the extruder at higher volume flows. However, the residence time distribution is more important than the average because particles can remain in the extruder for significantly different lengths of time. This explains why cleaning is seemingly less effective at lower volume flows, even though the cleaning rates are higher. The correlations with values A_1 and A_2 are what make the difference here. This demonstrates that, while efficiency and cleaning kinetics can be described quantitatively, describing the resulting effectiveness requires considering the absolute values and analyzing the remaining slurry on the screws. Hereby, the highest flow rate results for the lowest amount of slightly more than 0.3 g compared to 0.6 g for the lowest flow rate.

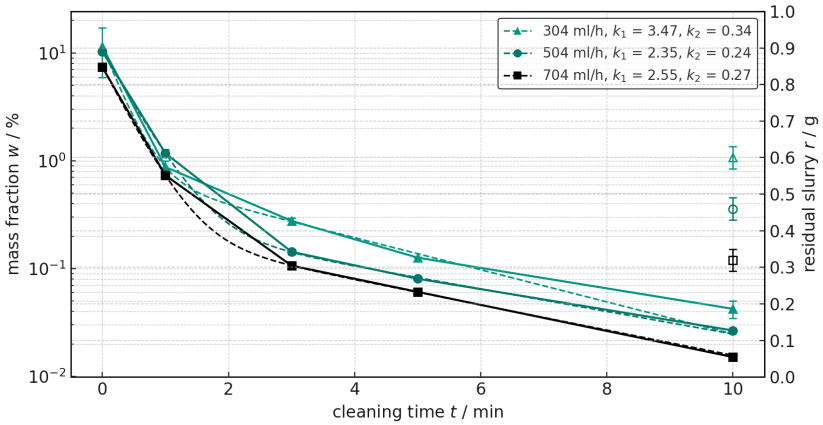

Figure 8. Influence of the volume flow on the cleaning performance with demineralized water at 500 rpm. Error bars indicate the standard deviation of triplicate cleaning experiments. Dashed lines show the fitted cleaning kinetic model.

The high value of k_1 at 304 mL/h shows that the cleaning process is slightly more efficient in the beginning, but the curve reaches a certain plateau earlier, which means that the efficiency decreases rapidly. Factors such as flow rate, turbulence and dwell time play a crucial role. At a lower flow rate, the liquid has a longer contact time with the surfaces, resulting in a faster initial cleaning effect, which explains the higher k_1 value. At the same time, the lower flow rate can lead to a buildup of contamination in certain areas or to residues that are more difficult to remove. This explains the higher residue levels found at the end that are decreasing with increasing flow rate.

3.5. Influence of Temperature

To investigate the cleaning process at elevated temperature, all zones of the extruder were heated to 90 °C. In addition, the screws were cleaned with deionized water at a moderate flow rate of 556 mL/h and a screw speed of 500 rpm. The sample water with the anode slurry residue, taken at the extruder outlet, had a measured temperature of about

50 °C. The cleaning temperature otherwise used is 20 °C, and cleaning with deionized water is also used for comparison in this chapter.

The results of the analysis of the influence of temperature are shown in Figure 9. When cleaning with deionized water at 50 °C, the initial mass ratio is 7.102%, which is similar to the value for cleaning at 20 °C. However, the reduction in the mass ratio over time is much faster, so that after one minute it is well below 1% at 0.536% and after three minutes it is already below 0.1% at 0.096%. In the final phase, the mass ratio continues to decrease and finally reaches 0.020% after ten minutes, so that the mass ratio at the normal cleaning temperature is approximately twice as high. This is also confirmed by comparing the cleaning rate k_1 at the beginning of 2.94 to the cleaning rate of 2.05 at room temperature.

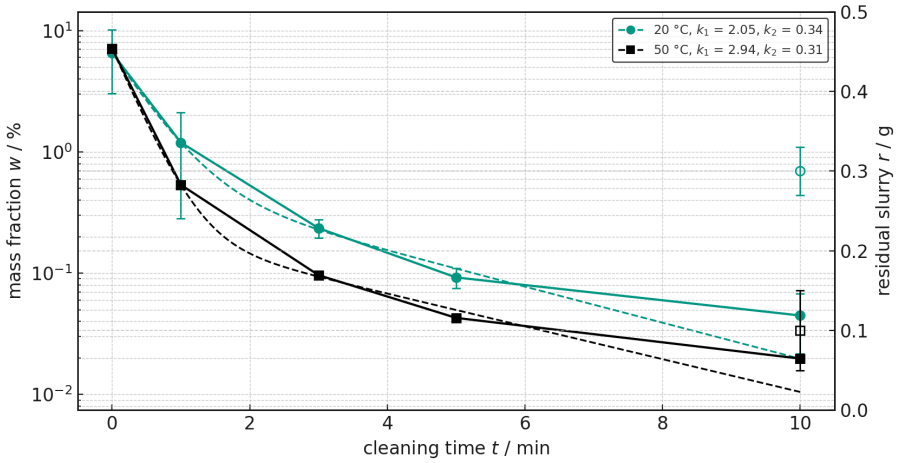

Figure 9. Influence of temperature on cleaning performance with demineralized water at 500 rpm and 556 mL/h. Error bars indicate the standard deviation of triplicate cleaning experiments. Dashed lines show the fitted cleaning kinetic model.

At higher temperatures, the deionized water is more effective in removing anode slurry residues, as evidenced by the faster and greater reduction in mass fraction over the entire cleaning time. At elevated temperatures, water becomes less viscous, improving the rinsing effect. At the same time, the viscosity of the residual slurry decreases, making it easier to wash out. Furthermore, CMC is water-soluble but swells slowly at room temperature. Higher temperatures increase the dissolution and swelling rates, causing binder residues to detach more quickly. Additionally, the surface tension of water decreases with temperature, resulting in better wetting of metal surfaces in the extruder. This means that remaining deposits are dissolved more effectively. This effect is confirmed by the gravimetrically determined residual slurry of 0.1 g at elevated temperature, compared to 0.3 g at room temperature.

Since cleaning with granules is state of the art in polymer processing using extruders, tests have also been carried out with cleaning granules after slurry production, but these require a temperature of over 150 °C. This preheating causes the residual slurry in the extruder chamber to dry out and harden, making an effective cleaning process impossible. In addition, the use of high temperatures in the extruder chamber should be avoided because, depending on the composition of the formulation, premature evaporation of the solvent or degradation of the binders could occur. Either scenario would be fatal to a flexible and automated production and cleaning process.

3.6. Overall Discussion

Comparing the cleaning efficiency of various parameters, the cleaning rate and the residual slurry remaining on the twin screws after cleaning were compared before. The

parameters studied included temperature, screw speed, volume flow and the type of detergent used. These measurements provide an insight into the effectiveness of different cleaning conditions, further supported by the plotted cleaning profiles obtained from the data. Table 1 summarizes the final measured value after each cleaning process and adds a calculation of the cleaning time until 0.01% residue is achieved. The aim is to illustrate the confirmation of taking two regimes into consideration. Hereby, the cleaning rate is discussed in terms of the remaining mass fraction after ten minutes and the predicted time to reach 0.01% concerning the efficiency. Additionally, the effectiveness must be examined in relation to the residual slurry.

Table 1. Final overview after completion of the cleaning process and calculated cleaning time until 0.01% residue.

Experiment	Mass Fraction in % After 10 min	Predicted Time to 0.01% in min
Deionized Water	0.045	10.34
Ethanol	0.078	34.19
CB 100	1.385	21.30
COSA™ CIP 96	0.166	Model implausible
screw speed (200 rpm)	0.038	13.32
screw speed (1000 rpm)	0.023	14.51
volume flow (304 mL/h)	0.042	12.64
volume flow (504 mL/h)	0.027	13.77
volume flow (704 mL/h)	0.015	11.67
Temperature (20 °C)	0.045	11.99
Temperature (50 °C)	0.020	10.16

Taking into account a free volume of 36.53 cm^3 for our screw configuration in the extruder chamber and a density of our anode suspension of approximately 1.3 g/cm^3, the extruder conveys most of the volume in the process chamber during processing without any further addition of material. Under the assumption of a fully filled extruder chamber results a slurry weight of 47.49 g which demonstrates that the remaining slurry is comparatively low by weight but clearly visible. This is confirmed qualitatively by comparing the values and shows that not all solvents are compatible and that the mechanical and thermal effects are dominant.

Residual slurry measurements and cleaning curves consistently demonstrate the significant impact of temperature, screw speed, and flow rate on cleaning efficiency. To make additional estimations, we approximated the kinetic model to predict the time, in minutes, until the remaining mass in the extruder is reduced to 0.01%. These results confirm previous findings that higher temperatures, slower long-term speeds, and higher cleaning medium volume flows optimize cleaning kinetics as they align with the mass fractions after ten minutes of cleaning. The fastest times are achieved in each case, as evidenced by the efficiency and effectiveness. Further evidence is provided by the lower residual slurry value on the twin screws. Among the cleaning agents tested, ionized water was the most effective, followed by CB100 and ethanol. A detailed analysis of these factors, supported by experimental data, provides valuable insights into optimizing the cleaning process for continuous dispersion.

For a final comparison for potential contamination with a cathode suspension that has a equally measured density of 1.3 g/cm^3, a mass fraction of 0.02% results in a residual weight of 0.95 g contaminated mass that is remaining after a cleaning process of 10 min, for a worst case scenario. Taking into account that a sample container has a volume of 50 mL and assuming that the remaining cathode suspension would contaminate the anode

paste, the worst-case scenario would result in contamination of 0.015%. All of this assumes that the cathode material would continue to adhere to the screw elements and would not change during the subsequent anode processing. This influence must now be validated in terms of electrochemistry.

3.7. Analysis of Cross-Contamination

Determining the effects of potential contamination during the mixing step requires investigating the resulting cell performance in terms of electrochemical properties. Due to the occurrence of unpredictable short circuits at the start of the 100-cycle test or during the test itself when contamination levels were too high, it has not yet been possible to identify a limit value for completed cleaning based solely on specific capacity data.

Therefore, an initial close examination was conducted to compare the discharge curves of an anode half-cell with those of a contaminated anode half-cell containing 8.5 wt% NMC. The results are shown in Figure 10a,b. Voltage over capacity was plotted for over 20 cycles. The sequence began with C/20, changed to C/10, and then concluded with C/5. During the first cycle, a passivation layer called solid electrolyte interface (SEI) forms on the anode when the electrolyte comes into contact with the first current. This layer protects the anode from further reactions with the electrolyte, thereby stabilizing the battery. However, if the SEI layer grows too thick over time, it leads to capacity loss and increased internal resistance of the battery. Thus, the SEI layer is an important yet problematic component. Thus, the first step is an irreversible process.

As shown in Figure 10a, the discharge curve in the first cycle of the reference anode is significantly longer, as the lower C-rate results in a slower cycle. The other curves do not show any gradations or discrepancies, such as undesirable side reactions. Thus, delithiation proceeds properly for the reference anode. A large difference in the first charging cycle is clearly visible when the reference is compared to the contaminated cell in Figure 10b. When the voltage falls below approximately 0.7 V, there is a sudden increase in voltage. This spike is an activation or side reaction artifact caused by the NMC particles on the anode. Therefore, lithiation of NMC occur simultaneously on the contaminated anode.

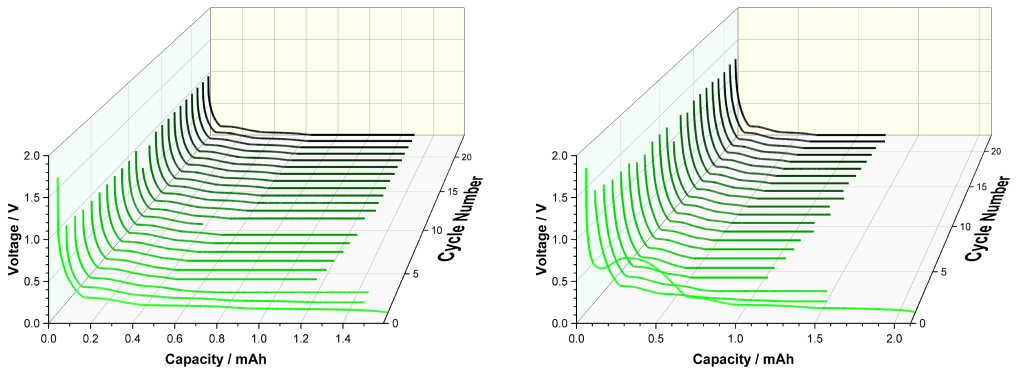

(**a**) (**b**)

Figure 10. Galvanostatic Cycling in 3D representation: voltage vs. capacity over several cycles in order to describe the discharge curves. (**a**) Anode half-cell as reference. (**b**) Anode half-cell contaminated with NMC.

Since NMC-contaminated anode half-cells led to a short circuit within a very short time when the contamination exceeded 12 wt%, LFP-contaminated anode half-cells were tested in parallel. A gradual increase in contamination was investigated. In this case, a significantly higher degree of contamination was achieved, presumably due to the considerably finer PSD of the LFP active material. The coin cells were cycled at C/10. A

total of 100 cycles were performed, nevertheless, no reproducible information on longevity or performance as a function of contamination could be obtained. Thus, the decisive electrochemical analysis comparison was performed in the first cycle.

The delithiation process undergoes several stages. Figure 11a shows the voltage curve as a function of specific capacity during the discharge of an anode half-cell. These describe the intercalation processes during delithiation and can be divided into four characteristic stages that correspond to the well-known staging sequence already described in previous studies: $LiC_6 \rightarrow LiC_{12} \rightarrow LiC_{18} \rightarrow LiC_{24} \rightarrow C$ [41].

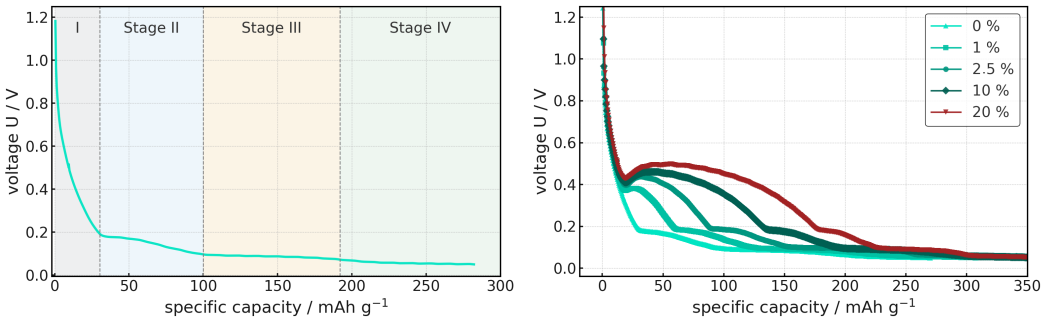

(**a**) (**b**)

Figure 11. Voltage curve of the delithiation of an anode half-cell over the specific discharge amount is shown. The graph shows the first discharge cycle. (**a**) Four stages of discharge of an anode half-cell as a reference. (**b**) Anode half-cell gradually contaminated with LFP from 0 wt% to 20 wt%.

Each of these stages is characterized by a typical potential plateau in the voltage curve and reflects structural rearrangements of the intercalation system. In the initial delithiation phase, lithium departs the fully occupied intercalation sites. This stage is characterized by a relatively steep voltage drop, as the lithium concentration in the graphite layers decreases abruptly. The associated plateau is comparatively short and thermodynamically stable, but reacts strongly to ohmic losses. As delithiation progresses, the Li occupancy density for the second stage decreases. In this stage, there is a significant drop in potential, which is determined by the coexistence of two phases, LiC_{12} and LiC_{18}, that describe the lithium stoichiometry in graphite. The process is increasingly limited by diffusion and interfacial kinetics. In the third phase, only part of the graphite layers are occupied by lithium. The plateau becomes flatter and is more strongly dominated by kinetic effects, as the Li transport paths are lengthened and the exchange current density at the interfaces decreases. The contribution to the total capacity is significant, but delithiation proceeds more slowly. The final delithiation stage corresponds to the removal of weakly bound residual lithium from the graphite layers. Thermodynamically, this results in a flat potential curve at low capacity. The fourth phase is characterized by a flat potential curve at low capacity.

These four stages were examined analogously for the contaminated cells, as shown in Figure 11b. It was found that the electrochemical discharge behavior of the graphite half-cells changes significantly with increasing LFP contamination. While the reference electrode without impurities clearly exhibits the characteristic potential plateaus of the graphite staging sequence, these plateaus become significantly shorter even with low LFP content.

At around 1–2.5 % contamination, the plateaus appear increasingly sloped and lose their horizontal shape. This indicates that the lithium is primarily absorbed by the contaminated cathode material in the half-cell anode, meaning that the lithium ultimately intercalates with the graphite. This additional accumulation of lithium causes a significant increase in voltage. The required end-of-charge voltage for LFP is approximately 3.6 V, which is never reached in the anode half-cell. Therefore, after the first cycle, the contam-

inated LFP acts as inert material in the cell, which further hinders ion transport. With 10 wt% and 20 wt% LFP content, this effect increases even more, as much more lithium is preferentially absorbed by the LFP in the first step, and this absorption is thus distributed over a wider voltage range. Thus, the transitions between stages are distorted, and plateaus are barely recognizable. This results in limiting electronic and ionic transport.

For a more in-depth electrochemical analysis of the contaminated half-cells, dQ/dU analyses were also performed. This differential capacity analysis is an established method for visualizing phase transformations and transitions within intercalation electrodes. Steps, plateaus, or breaks in the voltage curve appear as distinct peaks in the dQ/dU representation, which can be directly assigned to the phase boundaries of the graphite staging reactions. This allows the method to provide a much more precise analysis of the transition areas, the phases involved, and their relative proportions.

Figure 12 illustrates the electrochemical analysis of the various degrees of contamination, which, analogous to Figure 11 describing the delithiation curves, increase successively from a plain anode half-cell to a contamination rate of 20 wt% LFP. The diagram describes how the capacity of a cell changes as a function of voltage, which is used to investigate phase-specific reactions and degradation mechanisms. The ordinate describes the capacity density per voltage unit and explains how much charge is stored or discharged for a given voltage change. The abscissa describes the voltage of the battery relative to the lithium reference and thus indicates the state of discharge.

The curves from the first discharge cycle are shown, as an anomaly also occurs only in the first cycle. A sharp increase in dQ/dU below 0.5 V is a critical sign of unwanted reactions, from which capacity losses can be predicted. Possible causes for this are higher internal resistance, an unstable SEI layer, or electrolyte decomposition, which can result in a short circuit. Furthermore, lithium plating occurs preferentially below 0.5 V, which electrochemically confirms cross-contamination. Lithium plating leads to an accumulation of Li ions on the electrode, from which dendrites can grow through the electrolyte. As soon as these come into contact with the separator, a short circuit occurs, stopping the cycling of the cell.

The dQ/dU analyses illustrate the influence of LFP contamination on the delithiation of graphite. While the reference electrode without foreign matter shows pronounced and sharply defined peaks that can be assigned to the classic staging transitions, these characteristics are increasingly attenuated and broadened even at low contamination levels. At 2.5 wt% LFP, the peaks appear less intense and partially split, indicating a growing inhomogeneity of the reaction fronts. At 10 wt% and 20 wt%, the transitions are severely faded, and peaks that were originally separate merge, especially in the range of 0.4–0.5 V, where transport limitations dominate, which is why the dQ/dU curve is characterized by undefined signal areas and irregular deflections.

Based on the electrochemical analysis in Figure 12, an indicator can also be identified here in the first cycle, whereby even slight contamination of up to 2.5 wt% did not lead to any decrease in capacity or premature failure of the cell over 100 cycles. The presumed cause here is the formation of the SEI layer and the associated irreversible lithium deposition. This results in a large amount of charge being accumulated without any significant change in voltage, resulting in the high dQ/dU peak. The higher the contamination, the higher the peak, which shows a maximum point in the other charge direction at a contamination of 20 wt% LFP. Nevertheless, although these indicators show a clear influence of contamination on the electrochemical properties, they do not provide any information about the effects on the service life or performance of a longer-running cell. This has provided valuable electrochemical insights and quantifications on contaminated coin cells.

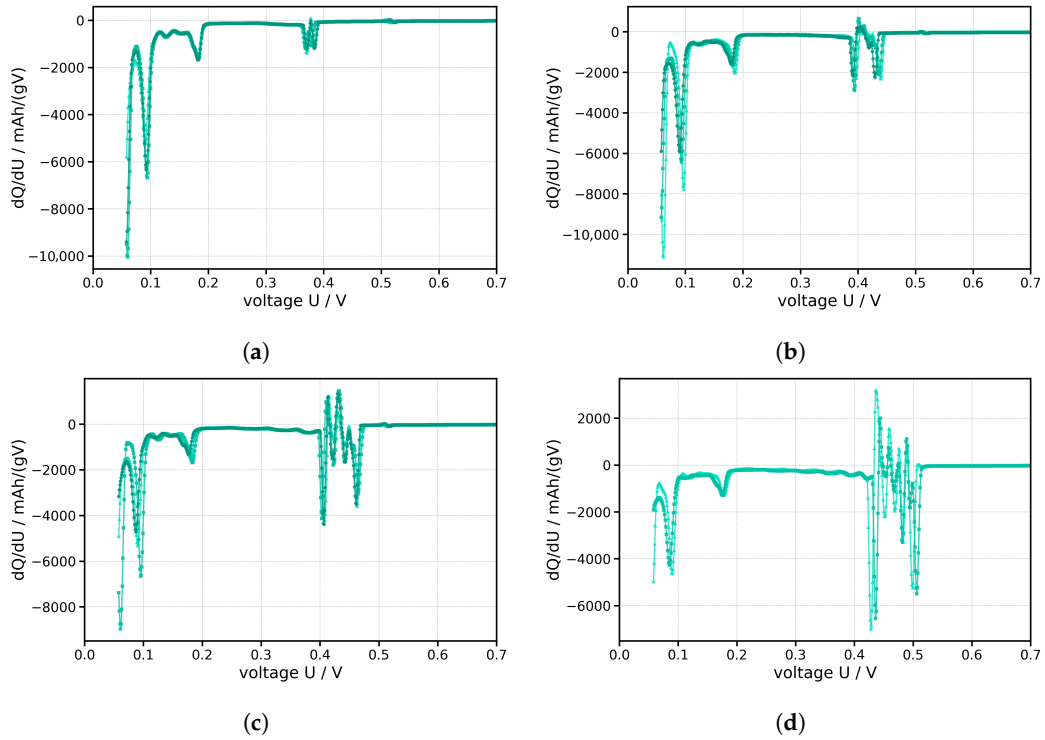

Figure 12. Electrochemical analysis of contaminated anode half-cells in the first cycle of cycling. (**a**) Anode half-cell as reference. (**b**) Anode half-cell contaminated with 2.5% LFP. (**c**) Anode half-cell contaminated with 10% LFP. (**d**) Anode half-cell contaminated with 20% LFP.

4. Conclusions

This work investigated the continuous production of anode slurry and its subsequent cleaning in a laboratory extruder, where the anode slurry was always produced according to a fixed recipe. The focus of this work was to investigate the optimum conditions for cleaning within the extruder and the resulting anode slurry residues to ensure a flexible and intelligent production of battery slurry. The influence of the four parameters of Sinner's circle was investigated to assess the effectiveness and efficiency of the cleaning process. All cleaning samples were measured by UV-Vis spectroscopy. Based on Lambert–Beer's law, a calibration curve was constructed using reference samples and a univariate linear regression to calculate the concentration or mass fraction of the sample remaining after the absorption measurement.

Deionized water proved to be the most effective cleaning medium, removing slurry fastest while avoiding additional safety concerns. Also, it acts as a solvent for the production of anode slurry. High initial screw speeds enhanced slurry detachment through stronger mechanical action, whereas lower speeds toward the end enabled more uniform deep cleaning. Despite the influence of residence time distribution on the apparent cleaning rate, increased flow rates further improved residue removal by flushing out more material in less time. Elevated temperatures likewise enhanced cleaning efficiency by accelerating slurry dissolution and detachment, as long as drying effects were avoided.

Regarding the electrochemical analysis of higher contamination levels, it was demonstrated that valuable information can be obtained during the initial charging cycle to determine the extent of contamination of the half-cell. Due to a certain charging voltage of the cathode material, which is never reached in an anode half-cell, the lithium primarily accumulates on the contaminated cathode material and then remains as inert material. Thus, increased contamination results in strong limitations of electronic and ion diffusion.

However, it was possible to demonstrate that, after five minutes, less than 0.1% slurry remained in almost every cleaning test. In terms of contamination levels, this would

not significantly impact battery performance but would promote long-term degradation mechanisms, such as lithium plating. Despite this, with sufficient time, the extruder can fully exploit its advantages over batch processing and significantly reduce the overall cleaning time.

In conclusion, this study has provided valuable insights into the continuous cleaning of anode slurry. It clearly shows that time, as well as thermal and chemical effects, greatly influence cleaning kinetics. Additionally, the self-cleaning effect of the twin-screw extruder has been confirmed. To optimize dwell time, cleaning should be carried out at the lower screw speed in the end with a high volume flow of cleaning medium that corresponds to the solvent of the intended slurry. Finally, the remaining materials should be removed from the extruder quickly and efficiently to ensure high quality and reproducibility of the upcoming formulation change. Nevertheless, testing these recommendations on industry-scale production lines is necessary to validate the experiments and quantify the economic efficiency.

Author Contributions: Conceptualization, K.R. and N.G.; data curation, K.R. and N.G.; formal analysis, K.R.; methodology, K.R.; software, K.R. and N.G.; validation, K.R.; investigation, K.R., F.Ö., N.G. and E.S.; resources, H.N.; writing—original draft preparation, K.R.; writing—review and editing, F.R.; visualization, K.R.; supervision, H.N. and F.R.; project administration, F.R.; funding acquisition, H.N. All authors have read and agreed to the published version of the manuscript.

Funding: This research was funded by BMBF in the project IntelliPast with the funding reference: 03XP0343A.

Data Availability Statement: Research data is available upon reasonable request.

Acknowledgments: We, the authors, express our sincere thanks to Thermo Fisher Scientific and Annika Völp for providing the extruder system and the support needed to carry out the respective experiments. We also thank the Thin Film Technology Institute at KIT for assistance in analyzing the particle size distributions. Finally, we thank Ulrike Kaufmann from the Institute for Applied Materials at KIT for her support with the SEM images, Marvin Winkler for his assistance with the UV-Vis measurements, and Bernhard Hochstein for his feedback on the rheological measurements. Special thanks also extend to Johann Chable for his support in realizing the cell construction, as well as to Anna Smith for her feedback and technical expertise.

Conflicts of Interest: The authors declare no conflict of interest.

Abbreviations

The following abbreviations are used in this manuscript:

CB	Carbon Black
CIP	cleaning-in-place
CMC	Carboxymethyl cellulose
LFP	Lithium Iron Phosphate
NMC	Lithium Nickel Manganese Cobalt Oxide
NMP	N-methylpyrrolidone
PSD	Particle Size Distribution
RFE	Recursive Feature Elimination
SBR	Styrene-butadiene rubber
SEI	Solid Electrolyte Interphase
SEM	Scanning Electron Microscope
UV–Vis	Ultraviolet–Visible Spectroscopy

Appendix A

Table A1. Fit parameters for different cleaning methods.

Cleaning Procedure	A_1	k_1	A_2	k_2	R^2
Deionized Water	5.9660	2.0499	0.6022	0.3418	0.99997
CB 100	6.2367	22.8841	4.3600	0.1145	0.99979
Ethanol	4.2590	6.0646	0.1170	0.0420	0.99999
Cosa CIP 96	11.6418	1.6864	0.0587	−0.0732	0.99998
screw speed—200 rpm	9.3668	2.4247	0.4342	0.2831	0.99999
screw speed—1000 rpm	2.8276	2.5669	0.1004	0.1590	0.99999
volume flow—304 mL/h	10.7061	3.4710	0.7635	0.3430	0.99999
volume flow—504 mL/h	10.0625	2.3512	0.2747	0.2407	0.99999
volume flow—704 mL/h	7.1507	2.5538	0.2319	0.2694	0.99999
temperature—20 °C	5.9660	2.0499	0.6022	0.3418	0.99997
temperature—50 °C	6.8661	2.9402	0.2358	0.3111	0.99999

References

1. Kim, T.; Song, W.; Son, D.Y.; Ono, L.K.; Qi, Y. Lithium-ion batteries: Outlook on present, future, and hybridized technologies. *J. Mater. Chem. A* **2019**, *7*, 2942–2964. [CrossRef]
2. Kwade, A.; Haselrieder, W.; Leithoff, R.; Modlinger, A.; Dietrich, F.; Droeder, K. Current status and challenges for automotive battery production technologies. *Nat. Energy* **2018**, *3*, 290–300. [CrossRef]
3. Kaiser, J.; Wenzel, V.; Nirschl, H.; Bitsch, B.; Willenbacher, N.; Baunach, M.; Schmitt, M.; Jaiser, S.; Scharfer, P.; Schabel, W. Process and Product Development of Electrodes for Lithium-Ion Cells. *Chem. Ing. Tech.* **2014**, *86*, 695–706. [CrossRef]
4. Wenzel, V.; Nirschl, H.; Nötzel, D. Challenges in Lithium-Ion-Battery Slurry Preparation and Potential of Modifying Electrode Structures by Different Mixing Processes. *Energy Technol.* **2015**, *3*, 692–698. [CrossRef]
5. Weber, M.; Mayer, J.K.; Kwade, A. The Carbon Black Dispersion Index DICB: A Novel Approach Describing the Dispersion Progress of Carbon Black Containing Battery Slurries. *Energy Technol.* **2023**, *11*, 2201299. [CrossRef]
6. Bauer, W.; Nötzel, D.; Wenzel, V.; Nirschl, H. Influence of dry mixing and distribution of conductive additives in cathodes for lithium ion batteries. *J. Power Sources* **2015**, *288*, 359–367. [CrossRef]
7. Weber, M.; Moschner, R.; Kwade, A. Modifying the Network Structures of High Energy Anodes for Lithium-Ion Batteries through Intensive Dry Mixing. *Energy Technol.* **2022**, *11*, 2200852. [CrossRef]
8. Schilde, C.; Mages-Sauter, C.; Kwade, A.; Schuchmann, H. Efficiency of different dispersing devices for dispersing nanosized silica and alumina. *Powder Technol.* **2011**, *207*, 353–361. [CrossRef]
9. Wenzel, V.; Moeller, R.S.; Nirschl, H. Influence of Mixing Technology and the Potential to Modify the Morphological Properties of Materials used in the Manufacture of Lithium-Ion Batteries. *Energy Technol.* **2014**, *2*, 176–182. [CrossRef]
10. Grießl, D.; Adam, A.; Huber, K.; Kwade, A. Effect of the Slurry Mixing Process on the Structural Properties of the Anode and the Resulting Fast-Charging Performance of the Lithium-Ion Battery Cell. *J. Electrochem. Soc.* **2022**, *169*, 020531. [CrossRef]
11. Schmid, E.; Pertzel, T.O.; Nirschl, H.; Guthausen, G. Characterization of Flow with a V-Shaped NMR Sensor. *Sensors* **2024**, *24*, 6163. [CrossRef]
12. Mayer, J.K.; Almar, L.; Asylbekov, E.; Haselrieder, W.; Kwade, A.; Weber, A.; Nirschl, H. Influence of the Carbon Black Dispersing Process on the Microstructure and Performance of Li-Ion Battery Cathodes. *Energy Technol.* **2019**, *8*, 1900161. [CrossRef]
13. Dreger, H.; Bockholt, H.; Haselrieder, W.; Kwade, A. Discontinuous and Continuous Processing of Low-Solvent Battery Slurries for Lithium Nickel Cobalt Manganese Oxide Electrodes. *J. Electron. Mater.* **2015**, *44*, 4434–4443. [CrossRef]
14. Haarmann, M.; Grießl, D.; Kwade, A. Continuous Processing of Cathode Slurry by Extrusion for Lithium-Ion Batteries. *Energy Technol.* **2021**, *9*, 2100250. [CrossRef]
15. Meza Gonzalez, J.F.; Nirschl, H. Numerical Investigation of the Local Shear Rate in a Twin-Screw Extruder for the Continuous Processing of Li-Ion Battery Electrode Slurries. *Energy Technol.* **2023**, *11*, 2201517. [CrossRef]
16. Meza Gonzalez, J.F.; Nirschl, H.; Rhein, F. Continuous Anode Slurry Production in Twin-Screw Extruders: Effects of the Process Setup on the Dispersion. *Batteries* **2024**, *10*, 145. [CrossRef]
17. Otte, S.; Sufian, N.N.A.M.; Schabel, S.; Fleischer, J. Identification of Relevant Parameters for Traceability in the Continuous Mixing Process in Battery Cell Production. *Energy Technol.* **2024**, *12*, 2400493. [CrossRef]
18. Lee, B.M.; Gao, X.; Sung Kim, H.; Ryol Hwang, W. Flow modeling for conveying sections in a co-rotating twin-screw extruder based on energy dissipation rate for continuous mixing of lithium-ion battery slurries. *Chem. Eng. Sci.* **2023**, *281*, 119113. [CrossRef]

19. Otte, S.; Mayer, D.; Fleischer, J. Digitaler Zwilling zur Steuerungscodevalidierung/Digital Twin for control code validation in battery cell production. *WT Werkstattstech. Online* **2023**, *113*, 272–277. [CrossRef]
20. Abeykoon, C. Single screw extrusion control: A comprehensive review and directions for improvements. *Control Eng. Pract.* **2016**, *51*, 69–80. [CrossRef]
21. Thon, C.; Finke, B.; Kwade, A.; Schilde, C. Artificial Intelligence in Process Engineering. *Adv. Intell. Syst.* **2021**, *3*, 2000261. [CrossRef]
22. Martínez-de Pisón, F.J.; Pernía, A.V.; Blanco, J.; González, A.; Lostado, R. Control Model for an Elastomer Extrusion Process Obtained via a Comparative Analysis of Data Mining and Artificial Intelligence Techniques. *Polym.-Plast. Technol. Eng.* **2010**, *49*, 779–790. [CrossRef]
23. Kohlgrüber, K. *Co-Rotating Twin-Screw Extruders: Applications*; Carl Hanser Verlag GmbH & Co. KG: München, Germany, 2020. [CrossRef]
24. Hauser, G. *Hygienegerechte Apparate und Anlagen*; John Wiley & Sons: Hoboken, NJ, USA, 2012.
25. Kohlgrüber, K. *Co-Rotating Twin-Screw Extruders: Fundamentals*; Carl Hanser Verlag GmbH & Co. KG: München, Germany, 2019. [CrossRef]
26. Zheng, H.; Zhang, L.; Liu, G.; Song, X.; Battaglia, V.S. Correlationship between electrode mechanics and long-term cycling performance for graphite anode in lithium ion cells. *J. Power Sources* **2012**, *217*, 530–537. [CrossRef]
27. Edge, J.S.; O'Kane, S.; Prosser, R.; Kirkaldy, N.D.; Patel, A.N.; Hales, A.; Ghosh, A.; Ai, W.; Chen, J.; Yang, J.; et al. Lithium ion battery degradation: What you need to know. *Phys. Chem. Chem. Phys.* **2021**, *23*, 8200–8221. [CrossRef] [PubMed]
28. Chen, W.; Han, X.; Pan, Y.; Yuan, Y.; Kong, X.; Liu, L.; Sun, Y.; Shen, W.; Xiong, R. Defects in Lithium-Ion Batteries: From Origins to Safety Risks. *Green Energy Intell. Transp.* **2025**, *4*, 100235. [CrossRef]
29. Grabow, J.; Klink, J.; Benger, R.; Hauer, I.; Beck, H.P. Particle Contamination in Commercial Lithium-Ion Cells—Risk Assessment with Focus on Internal Short Circuits and Replication by Currently Discussed Trigger Methods. *Batteries* **2022**, *9*, 9. [CrossRef]
30. Löwe, R.; Smith, A. Contamination in LIB Pouch Cells Promoting Self-Discharge and Crosstalk. *Batter. Supercaps* **2024**, *7*, e202400368. [CrossRef]
31. Gao, Z.; Xie, H.; Yu, H.; Ma, B.; Liu, X.; Chen, S. Study on Lithium-Ion Battery Degradation Caused by Side Reactions in Fast-Charging Process. *Front. Energy Res.* **2022**, *10*, 905710. [CrossRef]
32. Weidemann, C. *Reinigungsfähigkeit von Filtermedien Mithilfe Kontinuierlicher und Pulsierender Strömung*; KIT Scientific Publishing: Karlsruhe, Germany, 2015.
33. Gordon, R.; Orias, R.; Willenbacher, N. Effect of carboxymethyl cellulose on the flow behavior of lithium-ion battery anode slurries and the electrical as well as mechanical properties of corresponding dry layers. *J. Mater. Sci.* **2020**, *55*, 15867–15881. [CrossRef]
34. Anlauf, H. *Wet Cake Filtration*; Wiley-VCH: Weinheim, Germany, 2019.
35. Winkler, M. Prozesstechnische Fraktionierung von Nanoskaligen Partikeln in Röhrenzentrifugen. Ph.D. Thesis, Karlsruhe Institute of Technology, Karlsruhe, Germany, 2023. [CrossRef]
36. Reynolds, C.D.; Hare, S.D.; Slater, P.R.; Simmons, M.J.H.; Kendrick, E. Rheology and Structure of Lithium-Ion Battery Electrode Slurries. *Energy Technol.* **2022**, *10*, 2200545. [CrossRef]
37. Kuratani, K.; Ishibashi, K.; Komoda, Y.; Hidema, R.; Suzuki, H.; Kobayashi, H. Controlling of Dispersion State of Particles in Slurry and Electrochemical Properties of Electrodes. *J. Electrochem. Soc.* **2019**, *166*, A501–A506. [CrossRef]
38. Borzutzki, K.; Börner, M.; Fromm, O.; Rodehorst, U.; Winter, M. Process–Structure–Property Correlations in Twin-Screw Extrusion of Graphitic Negative Electrode Pastes for Lithium Ion Batteries Focusing on Kneading Concentrations. *Batteries* **2025**, *11*, 299. [CrossRef]
39. Haberzettl, P.; Filipovic, N.; Vrankovic, D.; Willenbacher, N. Processing of Aqueous Graphite–Silicon Oxide Slurries and Its Impact on Rheology, Coating Behavior, Microstructure, and Cell Performance. *Batteries* **2023**, *9*, 581. [CrossRef]
40. Schilde, C.; Kampen, I.; Kwade, A. Dispersion kinetics of nano-sized particles for different dispersing machines. *Chem. Eng. Sci.* **2010**, *65*, 3518–3527. [CrossRef]
41. Bauer, M. Elektrische und Mechanische Verfahren zur Detektion von Alterungseffekten in Lithium-Ionen-Batterien. Ph.D. Thesis, Technische Universität München, München, Germany, 2017. [CrossRef]